Localization of electronic wave packets in H-2

J. Phys. B: At. Mol. Opt. Phys. **41** (2008) 074022 (6pp) doi:10.1088/0953-4075/41/7/074022

Localization of electronic wave packets in H_2

A Kirrander[1], Ch Jungen[2] and H H Fielding[1]

[1] Department of Chemistry, University College London, 20 Gordon Street, London WC1H 0AJ, UK
[2] Laboratoire Aimé Cotton du CNRS, Université de Paris-Sud, 91405, Orsay, France

E-mail: h.h.fielding@ucl.ac.uk

Received 17 December 2007, in final form 7 February 2008
Published 25 March 2008
Online at stacks.iop.org/JPhysB/41/074022

Abstract
We demonstrate localization of electronic wave packets in the coupled channels of rotating and vibrating H_2 molecules using phase-shaped excitation pulses. The dynamics of Rydberg wave packets and their controlled preparation has been studied in detail in hydrogenic systems. We report here on a more general situation, where the strong channel couplings require full shaping of the optical phase, rather than a linear or quadratic chirp which is often sufficient in hydrogenic systems, or sequences of pulses which can be applied to uncoupled Rydberg series. The complex excitation functions for the shaped pulses are calculated and illustrate the longer duration and the complicated transients of the excitation process compared to excitation by an unshaped reference pulse.

(Some figures in this article are in colour only in the electronic version)

1. Introduction

Wave packets have become ubiquitous. They have been studied in atoms [1], small molecules [2], proteins [3], optical lattices [4], ion traps [5] and semiconductor quantum wells [6]. Despite the wide range of physical systems, wave packet evolution displays quite universal features, including dephasing, collapses [7] and fractional and full revivals [8]. The controlled preparation and measurement of wave packets has emerged as an active field of research.

Wave packets in hydrogenic Rydberg atomic systems have been studied experimentally and theoretically over the past two decades. Typically, a coherent superposition of Rydberg states is excited by a short optical pulse. Initial work concerned the preparation of the wave packets and their subsequent evolution, with particular attention to the classical and quantum-mechanical features typically displayed by the wave packet [7–11]. Soon the focus moved to the creation of exotic wave packets, such as electronic gratings [12], Schrödinger's cat states [13] and sculpting of hydrogenic wave packets by feedback optimization [1]. An important role in this progress was played by ever-improving methods of characterization of the wave packets. Quantum holography enables measurement of both the amplitude and the phase of the wave packets [14–18], while methods such as state selective field ionization (SSFI) [19] and the optical Ramsey method [20] enable measurement of the amplitude, but not the phase, of the wave packet components.

The relatively simple single-mode dynamics of hydrogenic systems even allows for analytic design of wave packets under certain conditions, e.g. [21–25]. In this paper we extend the focus to the more general case of multimode dynamics, in our case in coupled Rydberg channels corresponding to different rotational states of the H_2^+ core states of the highly excited H_2 molecule. By shaping the phase profile of the excitation pulse we can shift particular features in the wave packet evolution to any chosen time. One context where such control is interesting is in time-domain (pump-dump) coherent control [26], where for instance the localization of a wave packet in a particular Franck–Condon region of a potential energy surface could be desirable. We also investigate the excitation dynamics for the phase-shaped optical pulses and draw some general conclusions about the sculpting of wave packets.

2. Theory

A time-dependent wave packet is a coherent superposition of several eigenstates that can be expressed as

$$|\Psi(r,t)\rangle = \sum_n c_n(t)\exp(-\imath E_n t)|\Psi_n(r)\rangle, \tag{1}$$

where each state n is characterized by an energy E_n and a wavefunction $|\Psi_n(r)\rangle$. In this paper, the wavefunction coordinate r corresponds to the radial coordinate of the Rydberg electron and t denotes the time. We use natural units (nu), in this case Rydberg units, where the Rydberg constant $\mathrm{Ry} = \hbar = e = 1$ (e is the charge of an electron). The conversion between Rydberg and atomic units (au) of energy is simply $E(\mathrm{nu}) = 2E(\mathrm{au})$. For general conversion purposes the Rydberg energy is given in units of $\hbar^2/2ma_0^2$ and Rydberg time in units of $2ma_0^2/\hbar$, where m is the electron mass and a_0 the Bohr radius. The dimensionless expansion coefficients $c_n(t)$ change during the excitation process, but remain constant afterwards. In the weak field regime, where first order perturbation theory can be used, the coefficients are given by

$$c_n(t) = \imath D_{ns}\mathrm{cef}(E_n, t). \tag{2}$$

D_{ns} are the dipole transition moments connecting the state n and the initial state s, and $\mathrm{cef}(E_n, t)$ is the complex excitation function [27–29], defined by

$$\mathrm{cef}(E_n, t) = \int_{-\infty}^{\infty} \mathrm{d}E\epsilon(E)\int_{T=-\infty}^{t} \mathrm{d}t'\,\mathrm{e}^{\imath(E_n-E)t'}, \tag{3}$$

where $\epsilon(E)$ is the Fourier transform of the optical excitation pulse $\epsilon(t)$. The complex excitation function as defined here has the dimension of an inverse length and is a measure of the interaction strength of the field at a particular energy and time. At the end of the excitation pulse it is proportional to the spectral profile of the pulse (including phase), i.e. $\mathrm{cef}(E_n, t \to \infty) = 2\pi\epsilon(E_n)$.

The energies, wavefunctions and dipole transition moments for H_2 are obtained using multichannel quantum defect theory (MQDT) [30]. A detailed description of MQDT in the context of time-dependent perturbation theory can be found in [31][3]. Here, we present the most important equations required for the calculation of discrete states. The wavefunctions and the bound energies are obtained by enforcing the correct boundary conditions for the wavefunction at large r. The wavefunction outside the immediate vicinity of the H_2^+ core (in the volume of space occupied by the Rydberg electron) is given by

$$|\Psi_n(r)\rangle = \frac{1}{r}\sum_{j=1}^{N}|j\rangle\sum_{\alpha=1}^{N}A_{\alpha n}U_{j\alpha}[f_j(r,E_n)\cos\pi\mu_\alpha - g_j(r,E_n)\sin\pi\mu_\alpha], \tag{4}$$

where N is the total number of channels, each channel defined by a particular vibrational, rotational and electronic state $|j\rangle$ of the H_2^+ core and the corresponding angular momentum and spin state of the Rydberg electron. The matrix $U_{j\alpha}$ is the frame transformation, $A_{\alpha n}$ are the channel-mixing coefficients and μ_α the short-range quantum defects. Finally $f_j(r, E_n)$ and $g_j(r, E_n)$ are the single-electron radial wavefunctions. The scattering of the excited electron from the core mixes the different channels, leading to complicated multimode dynamics. The probability density of the wave packet in channel j according to equation (1) is given by the square modulus of the projection on $|j\rangle$, i.e. $|\langle j|\Psi(r,t)\rangle|^2$. Finally, the dipole transition moment D_{ns} is calculated as

$$D_{ns} = \sum_{\alpha=1}^{N} D_{\alpha s}A_{\alpha n}, \tag{5}$$

where $D_{\alpha s}$ is the transition amplitude connecting the initial discrete state $|\Psi_s\rangle$ to each short-range channel α.

2.1. Localization

The evolution of the wave packet in equation (1) is, at each time t, a sum of complex vectors that rotate in the complex plane with angular frequency E_n (in Rydberg and atomic units $E_n = \omega_n$), much like the dials of an imaginary 'quantum clock'. The simple idea pursued here is to use the phase profile $\Phi(E)$ of the excitation pulse $\epsilon(E) = |\epsilon(E)|\exp(\imath\Phi(E))$, to set this clock, or equivalently, to determine the shape of the wave packet at a chosen target time t_f.

During a period T_{full}, corresponding to the revival time required for the wave packet to return to its original state *exactly*, the wave packet explores all the phase space available to it. A specific feature (e.g. a well-localized or multiply peaked wave packet) which occurs at a particular time t_s can be shifted to a target time t_f by the phase profile $\Phi(E)$ in the excitation pulse. The phase profile enters equation (1) as $\exp(\imath\Phi(E))$ through the expansion coefficients $c_n(t)$, as follows from equations (1)–(3). Hence, the phase profile is defined at each discrete energy E_n by

$$\Phi(E_n) = \mathrm{mod}(E_n(t_f - t_s), 2\pi). \tag{6}$$

This phase profile will, in general, have some arbitrary shape, but can be fitted to a smooth polynomial, which is important to yield the shortest possible excitation pulse. The observation that phase determines the trajectory of the wave packet through the available phase space, suggests a straightforward method of optimizing pulses in the weak field regime, with a linear search in time ($t \in [0, T_{\mathrm{full}}]$) in the phase space volume determined by the excitation amplitudes. The excitation phases then allow the localization of a particular feature, normally occurring at some time t_s, to a chosen target time t_f.

We connect briefly to single mode dynamics of a wave packet, which has been the focus of previous work [1, 14, 21, 22, 32]. This could, for instance, be a Rydberg electron in a hydrogenic atom or vibrations on a single potential energy curve in a diatomic molecule. We assume that the pulse is centred at the mean principal quantum number $\bar{n}$ and that states are approximately equidistant in energy (i.e. there is an absence of interloper states from coupled channels) so that we can make a short Taylor expansion in n around $\bar{n}$ ($\Delta n = n - \bar{n}$),

$$E_n = E_{\bar{n}} + E_{\bar{n}}^{(1)}\Delta n + \frac{1}{2}E_{\bar{n}}^{(2)}\Delta n^2 + \frac{1}{6}E_{\bar{n}}^{(3)}\Delta n^3, \quad \text{with} \quad E_{\bar{n}}^{(k)} = \frac{\partial^k E_{\bar{n}}}{\partial \bar{n}^k}, \tag{7}$$

truncated at third order. This expansion defines three time scales for the revivals in equation (1), namely $T_{\mathrm{cl}} = 2\pi/E_{\bar{n}}^{(1)}$,

[3] In this reference all MQDT derivations are in Rydberg units.

$T_{\rm rev} = 2\pi/E^{(2)}_{\bar{n}}$ and $T_{\rm sup} = 2\pi/E^{(3)}_{\bar{n}}$, such that $T_{\rm sup} \gg T_{\rm rev} \gg T_{\rm cl}$. Note that some authors define $T_{\rm rev} = 4\pi/E^{(2)}_{\bar{n}}$ [33]. Furthermore, fractional revivals will occur, corresponding to subgroups of vectors coming into phase [8, 33] and creating multipeaked structures such as the electronic grating in [12]. By inserting the expansion of energies in equation (7) in the phase evolution in equation (1), we see immediately how the phase evolution can be controlled analytically by appropriate linear, quadratic and cubic chirps in the excitation pulse [21, 32].

Specifically, in a hydrogenic Rydberg system energies are given by $E_n = -1/n^2$. This leads to $T_{\rm cl} = \pi\bar{n}^3$, $T_{\rm rev} = \pi\bar{n}^4/3$ and $T_{\rm sup} = \pi\bar{n}^5/12$ in Rydberg units (in atomic units $E_n = -1/2n^2$ and hence $T_{\rm cl} = 2\pi\bar{n}^3$, $T_{\rm rev} = 2\pi\bar{n}^4/3$ and $T_{\rm sup} = \pi\bar{n}^5/6$). Accounting for the quantum defect, energy levels are shifted by approximately $\Delta E = 2\mu/\bar{n}^3$, which leads to an additional linear phase evolution of $2\pi\mu t/T_{\rm cl}$ [23–25, 34, 35]. This illustrates elegantly how the quantum defect shifts both energies and equivalently phases, and fits nicely with the semiclassical picture of core-electron recollisions occurring with a period $T_{\rm cl}$.

3. Calculation

The present calculations concern one-photon excitation from the rotationless ground level $J'' = 0$, which leads to $N = J = 1$ angular momentum negative parity singlet states with a Rydberg electron with predominantly $l = 1$ angular momentum. Thus only ion rotation levels with $N^+ = 0$ and 2 can be reached. We concentrate on a region of the H_2 spectrum dominated by two channels corresponding to the H_2^+ core states $|j = 1\rangle = |\upsilon^+ = 0, N^+ = 0\rangle$ and $|j = 2\rangle = |\upsilon^+ = 0, N^+ = 2\rangle$ [36], where υ^+ and N^+ are the vibration and rotation quantum numbers respectively and the electronic state of H_2^+ is $1s\sigma_g$ for both channels. The short-range interactions are given by quantum defects $\mu_{\alpha=1} = 0.203$ and $\mu_{\alpha=2} = -0.082$ in the eigenchannel picture. For further details on the MQDT model, see [31, 37].

We use a Gaussian optical excitation pulse, which can be written in the frequency domain as

$$\epsilon(E) = \epsilon_0\, \mathrm{e}^{-\alpha^2(E-E_0)^2}\, \mathrm{e}^{\imath\Phi(E)}, \tag{8}$$

where $\Phi(E)$ defines the phase profile and we use the rotating wave approximation. We discuss the pulse envelope first: ϵ_0 is the pulse amplitude, E_0 the central optical frequency, $\alpha = \tau_t/\sqrt{8\ln 2}$ and τ_t is the full width at half maximum (FWHM) pulse duration, defined for the intensity profile of the transform-limited pulse. The corresponding width in the frequency domain is $\tau_E = 4\ln 2/\tau_t$. The values used throughout are $\epsilon_0 = 1$, $E_0 = 124234.7$ cm^{-1} and $\tau_t = 0.5204$ ps ($\tau_E = 28$ cm^{-1}).

The phases $\Phi(E_n)$ of the excitation pulse are determined by a linear search in time $t \in [0, T_{\rm full}]$ against pre-defined target wave packets. The wave packet is evolved in time over the period $T_{\rm full}$, while its overlap with the target wave packets is checked. In the present calculation, $T_{\rm full} = 894.4$ ps. The phases which generate maximum overlap with the target are then shifted from their original time t_s to the target time $t_f = 10.0$ ps by equation (6). Finally, the resulting phases $\Phi(E_n)$ are fitted by a smooth spline function $\Phi(E)$, defined at all energies. The smoothness of the phase profile function $\Phi(E)$ is important to minimize the broadening of the pulse.

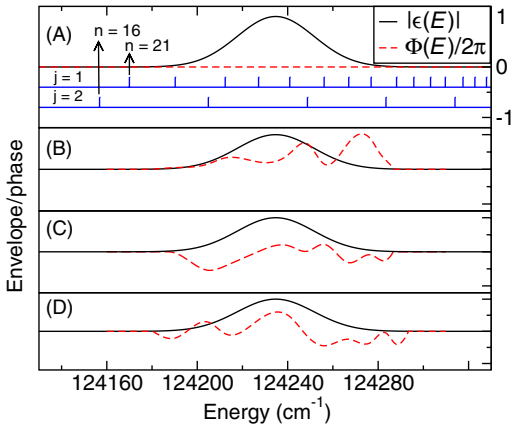

Figure 1. The pulse profile, including the envelope $|\epsilon(E)|$ and the phase profile $\Phi(E)$, as a function of energy (cm^{-1}) for the excitation pulses. The Gaussian envelope has the width $\tau_E = 28$ cm^{-1}, which corresponds to a duration $\tau_t = 0.5204$ ps (FWHM), and is centred at energy $E_0 = 124\,234.7$ cm^{-1} for all pulses. (*A*) The phase profile for the reference pulse A, $\Phi(E) \equiv 0$. Energy levels are indicated. Note that although we assign each energy level to a particular channel, the channel couplings lead to wavefunctions with substantial amplitude in both channels at each energy. (*B*) The phase profile for pulse B localizes the wave packet at the outer turning point in both channels. (*C*) Phase profile C maximizes the probability of the electronic wave packet in channel $j = 2$, while minimizing the probability in channel $j = 1$. (*D*) Phase profile D maximizes the probability of the electronic wave packet in channel $j = 1$, while minimizing the probability in channel $j = 2$.

Four pulses with the same pulse envelope, but different phase profiles are used in the calculations. Pulse A is a reference pulse with unshaped phase profile, $\Phi(E) \equiv 0$. The shaped pulses B, C and D are shown in figure 1. Pulse B corresponds to the wave packet being localized at the outer turning point in both channels, and pulses C and D localize the wave packet in channel $j = 2$ or $j = 1$ respectively, so that the probability of detecting the wave packet in that particular channel is maximal.

4. Results

The complex excitation functions (CEFs) for the four excitation pulses A, B, C and D described in section 3 are shown in figure 2. The CEFs give the amplitude and phase of the excitation throughout the excitation process as a function of time (ps) and energy (cm^{-1}). At large times, the amplitudes of all four CEFs are identical and proportional to the spectral profile of the pulse. On the other hand, the overall pulse duration and the complexity of the transients increases as the phase profile becomes more complicated. The CEF for the unshaped reference pulse in figure 2(a) reaches its limiting value in only 1 ps and has the fewest transient features (essentially a broadening around time $t = 0$ ps), while pulses B, C and D give rise to considerably more complicated CEFs

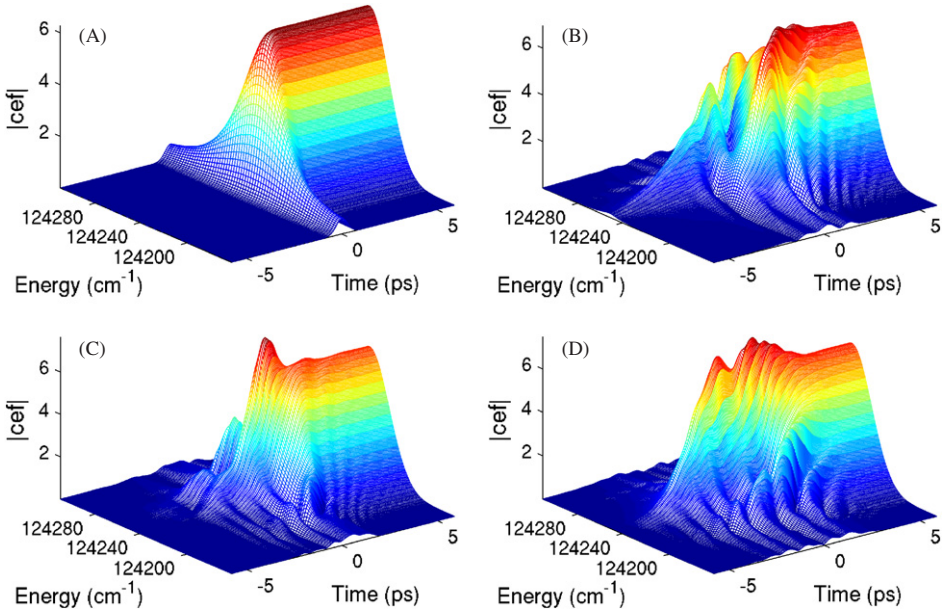

Figure 2. The amplitude of the complex excitation function, $|\mathrm{cef}(E, t)|$, as a function of time (ps) and energy (cm^{-1}) for the four excitation pulses with the same Gaussian envelope in the energy domain, but different phase profiles (A–D in figure 1, where A is the reference pulse).

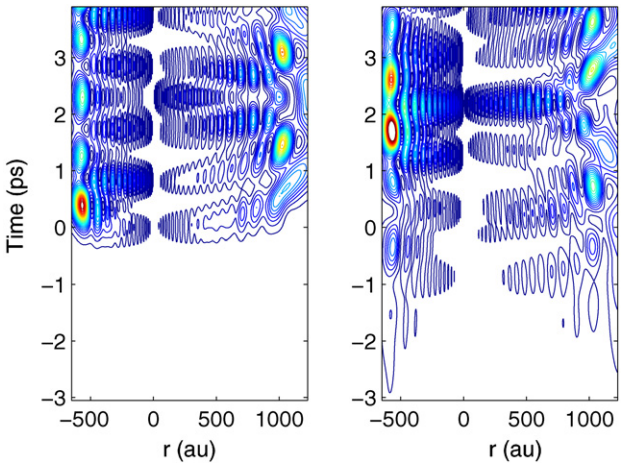

Figure 3. Comparison of the excitation process with the unshaped reference pulse A (left panel) and the phase-shaped pulse B (right panel). The contour plot shows the wave packet probability density $|\langle j|\Psi(r, t)\rangle|^2$ as a function of radial distance r (au) and time t (ps). Negative radial distances r correspond to the dynamics in channel $j = 2$, while positive radial distances correspond to channel $j = 1$. In both channels, the wave packet oscillates between the core ($r \approx 0$) and the outer turning point. For pulse A (left panel), the excitation at time $t \approx 0$ ps is almost instant and is quickly followed by free evolution of the wave packet. For pulse B (right panel), the excitation process with the shaped pulse begins already at times $t < -5$ ps, becomes discernible in the contour plot at times $t \approx -3$ ps and does not evolve freely until for times $t > 5$ ps.

and require 6 ps to 12 ps to reach their limiting values. Note also that the excitation with the shaped pulses is not uniform in time across the different energies and that some transient features, for instance in the CEF for pulse C in figure 2(c), have amplitudes that surpass the final excitation amplitude quite substantially.

The excitation dynamics for the reference pulse A and for pulse B is compared in figure 3. The almost instant excitation with the reference pulse is followed by free evolution of the wave packet. The overall dynamics follows the typical Rydberg pattern of oscillations between the core $r \approx 0$ and the outer turning point. Note that the wave packet in channel $j = 1$ has its outer turning point at larger distances. The outer turning point is given by $r_{\mathrm{cl}} = 2\bar{n}^2$, where $\bar{n}$ is the mean principal quantum number. This is $\bar{n}_1 = 24.5$ in channel 1 $\left(r_{\mathrm{cl}}^{(1)} = 1200\ \mathrm{au}\right)$ and $\bar{n}_2 = 17.5$ in channel 2 $\left(r_{\mathrm{cl}}^{(2)} = 615\ \mathrm{au}\right)$.

The effect of the coupling between the channels can be seen clearly in the oscillation period T_{cl}. This is, strictly speaking, only defined for a single (or uncoupled) channel that can be described by equation (7). In a system of two uncoupled channels, the different mean principal quantum number would give two separate time scales, $T_{\mathrm{cl}}^{(1)} = 2.2$ ps in channel $j = 1$ and $T_{\mathrm{cl}}^{(2)} = 0.8$ ps in channel $j = 2$. Here, due to the coupling between the channels, both time scales are present in both channels. The shorter time scale $T_{\mathrm{cl}}^{(1)}$ is immediately visible, while the longer period $T_{\mathrm{cl}}^{(2)}$ gives a modulation of the probability density, discernible in the free evolution of the pulse A wave packet for $t > 0.8$ ps.

The general features of the dynamics for pulse B in figure 3 are similar to pulse A, but the excitation of the wave packet with pulse B takes substantially longer. It begins already at times $t < -5$ ps, with the wave packet becoming visible in the contour plot at times $t \approx -3$ ps and free evolution of the wave packet does not ensue until times $t > 5$ ps. The dynamics during the excitation is not simply a muted version of the free wave packet dynamics, due to the transient structures visible in figure 2(b).

In figure 4, the wave packet probability density in both channels is shown for the unshaped reference pulse A and the three shaped pulses B, C and D in the vicinity of the target

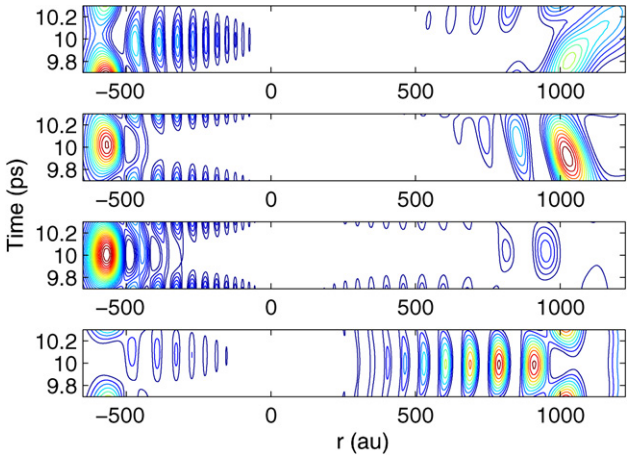

Figure 4. The wave packet probability density $|\langle j|\Psi(r,t)\rangle|^2$ in the two channels $j = 1$ and $j = 2$ around the target time $t_f = 10.0$ ps after excitation with reference pulse A and the shaped pulses B, C and D (see figure 1). The contour plots show the wave packet dynamics as a function of radial distance r (au) and time t (ps). Negative radial distances r correspond to the dynamics in channel $j = 2$, while positive radial distances correspond to channel $j = 1$. Pulse A (first panel) gives the unshaped wave packet. Pulse B (second panel) generates a wave packet localized close to the outer turning point in both channels. Pulse C (third panel) generates a wave packet with little probability density in channel $j = 1$ and most of the probability density localized at the outer turning point in channel $j = 2$. This corresponds to the molecule predominantly localized in the $N^+ = 2$ rotational state. Pulse D (fourth panel) generates a wave packet with most probability density in channel $j = 1$, which corresponds to the molecule predominantly localized in the $N^+ = 0$ rotational state.

time $t_f = 10.0$ ps. The optimization targets for pulses B, C and D are attained fairly well. Pulse B localizes the wave packet close to the outer turning points in both channels with a (0.60,0.40) distribution between the channels ($j = 1$, $j = 2$). The probability for each channel is obtained by integrating the channel-specific probability density $|\langle j|\Psi(r,t)\rangle|^2$ over the radial distance r at the target time. Pulse C gives a wave packet localized at the outer turning point in channel $j = 2$ with a (0.26,0.74) distribution. This corresponds to the molecule predominantly in the $N^+ = 2$ rotational state. Finally, pulse D localizes the wave packet in channel $j = 1$ with a (0.82,0.18) distribution between the two channels, which corresponds to the molecule being rather strongly localized in the $N^+ = 0$ state. In a channel perspective, the effective cancelling of amplitude in either channel is aided by the interloper states in each channel. The interlopers are an important aspect of the coupling between the two channels and one of the reasons why a simple linear chirp is insufficient to control timing in a general multimode system.

It is also interesting to quantify how stable the localization of the wave packets is. We do this by calculating the average probability distribution between the two channels averaged over a 0.6 ps time window, i.e. from $t = 9.7$ ps to $t = 10.3$ ps. The distributions thus obtained are (0.59,0.41) for pulse B, (0.31,0.69) for pulse C and (0.78,0.22) for pulse D. These distributions are quite similar to the distributions at the target time $t = 10$ ps given above, and indicate that the target waveforms are relatively stable over such a 0.6 ps time frame. This stability is entirely due to the natural time scales of the free wave packet evolution, since the target time is reached under field-free conditions.

5. Conclusions

This paper discusses the sculpting and optimization of wave packets. The excitation amplitudes determine the phase space volume available to the wave packet, while the phase evolution determines the trajectory of the wave packet through a given phase space. This suggests a straightforward method for optimizing pulses in the weak-field regime, with a linear search in time in the phase space volume determined by each set of excitation amplitudes. The excitation phases then allow the localization of a particular feature to a specific time. With recent advances in shaping of optical pulses [38] such arbitrary phase profiles are quite feasible. This may be useful for time-domain (pump-dump) coherent control [26], where for instance the localization of a wave packet in a particular Franck–Condon region of a potential energy surface is desirable. The analysis presented in this paper is based on the field-free evolution of wave packets and does not directly depend on the details of the excitation process. It could therefore be useful for strong field experiments if the excitation phases could be controlled and the duration of the shaped pulse kept short enough to allow for field-free evolution of the wave packet. Finally, the present work is part of our development of a complete theoretical toolkit to simulate and model coherent control and ultrafast experiments in Rydberg states of atoms and diatomic molecules using MQDT.

Acknowledgments

AK acknowledges a research fellowship from the Leverhulme Trust. ChJ and HHF thank the Royal Society for an International Joint Project Grant.

References

[1] Weinacht T C, Ahn J and Bucksbaum P H 1999 Controlling the shape of a quantum wavefunction *Nature* **397** 233
[2] Katsuki H, Chiba H, Girard B, Meier C and Ohmori K 2006 Visualizing picometric quantum ripples of ultrafast wave-packet interference *Science* **311** 1589
[3] Lee H, Cheng Y-C and Fleming G R 2007 Coherence dynamics in photosynthesis: protein protection of excitonic coherence *Science* **316** 1462
[4] Raithel G, Birkl G, Phillips W D and Rolston S L 1997 Compression and parametric driving of atoms in optical lattices *Phys. Rev. Lett.* **78** 2928
[5] Meekhof D M, Monroe C, King B E, Itano W M and Wineland D J 1996 Generation of nonclassical motional states of a trapped atom *Phys. Rev. Lett.* **76** 1796
[6] Steininger F, Knorr A, Stroucken T, Thomas P and Koch S W 1996 Dynamic evolution of spatiotemporally localized electronic wave packets in semiconductor quantum wells *Phys. Rev. Lett.* **77** 550
[7] Yeazell J A, M Mark and Stroud C R Jr 1990 Observation of the collapse and revival of a Rydberg electronic wave packet *Phys. Rev. Lett.* **64** 2007

[8] Yeazell J A and Stroud C R Jr 1991 Observation of fractional revivals in the evolution of a Rydberg atomic wave packet *Phys. Rev.* A **43** 5153
[9] Parker J and Stroud C R Jr 1986 Coherence and decay of Rydberg wave packets *Phys. Rev. Lett.* **56** 716
[10] Alber G, Ritsch H and Zoller P 1986 Generation and detection of Rydberg wave packets by short laser pulses *Phys. Rev.* A **34** 1058
[11] Henle W A, Ritsch H and Zoller P 1987 Rydberg wave packets in many electron atoms excited by short laser pulses *Phys. Rev.* A **36** 683
[12] Krause J L, Schafer K J, Ben-Nun M and Wilson K R 1997 Creating and detecting shaped Rydberg wave packets *Phys. Rev. Lett.* **79** 4978
[13] Noel M W and Stroud C R Jr 1996 Excitation of an atomic electron to a coherent superposition of macroscopically distinct states *Phys. Rev. Lett.* **77** 1913
[14] Schumacher D W, Hoogenraad J H, Pinkos Dan and Bucksbaum P H 1995 Programmable cesium Rydberg wave packets *Phys. Rev.* A **52** 4719
[15] Chen X and Yeazell J A 1997 Reconstruction of engineered atomic wave functions via phase-dependent population measurements *Phys. Rev.* A **56** 2316
[16] Weinacht T C, Ahn J and Bucksbaum P H 1998 Measurement of the amplitude and phase of a sculpted Rydberg wave packet *Phys. Rev. Lett.* **80** 5508
[17] Leichtle C, Schleich W P, Averbukh I Sh and Shapiro M 1998 Quantum state holography *Phys. Rev. Lett.* **80** 1418
[18] Averbukh I Sh, Shapiro M, Leichtle C and Schleich W P 1999 Reconstructing wave packets by quantum state holography *Phys. Rev.* A **59** 2163
[19] Gallagher T F, Humphrey L M, Cooke W E, Hill R M and Edelstein S A 1977 Field ionization of highly excited states of sodium *Phys. Rev.* A **16** 1098
[20] Noordam L D, Duncan D I and Gallagher T F 1992 Ramsey fringes in atomic Rydberg wave packets *Phys. Rev.* A **45** 4734
[21] Chen Xin and Yeazell J A 1998 Analytical wave-packet design scheme: control of dynamics and creation of exotic wave packets *Phys. Rev.* A **57** R2274
[22] de Araujo L E E, Walmsley I A and Stroud C R Jr 1998 Analytic solution for strong-field quantum control of atomic wave packets *Phys. Rev. Lett.* **81** 955
[23] Minns R S, Patel R, Verlet J R R and Fielding H H 2003 Optical control of the rotational angular momentum of a molecular Rydberg wave packet *Phys. Rev. Lett.* **91** 243601–1
[24] Verlet J R R, Stavros V G, Minns R S and Fielding H H 2002 Controlling the angular momentum composition of a Rydberg electron wave packet *Phys. Rev. Lett.* **89** 263004
[25] Minns R S, Verlet J R R, Watkins L J and Fielding H H 2003 Observation and control of dissociating and autoionizing Rydberg electron wave packets in NO *J. Chem. Phys.* **119** 5842
[26] Tannor D J and Rice S A 1985 Control of selectivity of chemical reaction via control of wave packet evolution *J. Chem. Phys.* **83** 5013
[27] Shapiro M 1990 Fundamental theory of photodissociation with pulses *Half Collision Resonance Phenomena in Molecules* (*AIP Conf. Proc.* vol 225) ed M Garcia-Sucre, G Raseev and S Ross (New York: AIP) p 230
[28] Shapiro M and Brumer P 2003 *Principles of the Quantum Control of Molecular Processes* 1st edn (New York: Wiley)
[29] Taylor R D and Brumer P 1983 Pulsed laser preparation and quantum superposition state evolution in regular and irregular systems *Faraday Discuss. Chem. Soc.* **75** 117
[30] Greene C H and Jungen Ch 1985 Molecular applications of quantum defect theory *Adv. At. Mol. Phys.* **21** 51
[31] Kirrander A, Fielding H H and Jungen Ch 2007 Excitation, dynamics and control of rotationally autoionizing Rydberg states of H_2 *J. Chem. Phys.* **127** 164301–1
[32] de Araujo L E E and Walmsley I A 2003 Analytic solution for quantum control of atomic and molecular wave packets *J. Opt. B: Quantum Semiclass. Opt.* **5** R27
[33] Averbukh I Sh and Perelman N F 1989 Fractional revivals: universality in the long-term evolution of quantum wave packets beyond the correspondence principle dynamics *Phys. Lett.* A **139** 449
[34] Carley R E, Boleat E D, Minns R S, Patel R and Fielding H H 2005 Interfering Rydberg wave packets in Na *J. Phys. B: At. Mol. Opt. Phys.* **38** 1907
[35] Fielding H H 2005 Rydberg wave packets in molecules: from observation to control *Annu. Rev. Phys. Chem.* **56** 91
[36] Herzberg G and Jungen Ch 1972 Rydberg series and ionization potential of the H_2 molecule *J. Mol. Spectrosc.* **41** 425
[37] Texier F and Jungen Ch 1999 Wave packets using generalized multichannel quantum-defect theory *Phys. Rev.* A **59** 412
[38] Weiner A M 2000 Femtosecond pulse shaping using spatial light modulators *Rev. Sci. Instrum.* **71** 1929